HOSTED BY

ELSEVIER

Available online at www.sciencedirect.com

ScienceDirect

Soils and Foundations 58 (2018) 1446–1457

SOILS AND FOUNDATIONS

www.elsevier.com/locate/sandf

Simplified analysis of cantilever diaphragm walls in cohesive soils

Enrico Conte, Antonello Troncone *

Department of Civil Engineering, University of Calabria, 87036 Rende, Cosenza, Italy

Received 4 January 2018; received in revised form 11 July 2018; accepted 9 August 2018
Available online 12 November 2018

Abstract

In this paper, a method is presented for a simplified analysis of cantilever diaphragm walls in cohesive soils under undrained and drained conditions. A rectilinear distribution of the net contact stresses that are not completely predetermined by the limit state is assumed at the soil-wall interface, consistently with the mechanism usually experienced by these structures. Simple equations are derived to readily calculate the contact stress distribution on the wall and the associated internal forces in the ultimate and service conditions. Moreover, these equations require few parameters as input data. Comparisons are carried out with a limit equilibrium method commonly used in design to show the usefulness of the proposed method for practical purposes.

Keywords: Earth pressure; Active pressure; Passive pressure; Retaining structures (**IGC**: E5/H2)

1. Introduction

Diaphragm walls are extensively employed as temporary and permanent retaining structures to provide a lateral support to an unstable soil mass owing to excavations. These structures can be cantilevered, usually when the retained height is relatively low, or anchored. The wall stability of cantilevered structures is essentially ensured by the passive resistance in front of the structure on the excavated side, and the embedment depth is designed to allow the development of this resistance. In addition, the structure has to be designed to resist the internal forces induced by the contact stresses, with the mechanical behaviour of the involved materials properly taken into account (Conte et al., 2013, 2015).

In many situations, the wall is constructed in clayey or silty soils. In these circumstances, the stress removal due to excavation induces negative excess pore water pressures that progressively dissipate with time. As steady state seepage conditions are approached, the dissipation of these pore pressures has a destabilising effect on the wall. By contrast, the movements of the wall may result in a significant increase in pore water pressure in the soil in front of the wall (on the excavated side), the dissipation of which leads in principle to an improvement of the wall stability. It is generally difficult to establish a priori which effect prevails and whether there is an increase or a reduction in the safety margin during the consolidation process (Lancellotta, 2002). Consequently, the designer should consider both outcomes by analysing the wall behaviour under undrained and drained conditions, especially in soft clays. An undrained analysis is especially important for temporary diaphragm walls.

Conventional calculations are based on the limit equilibrium method, in which the mechanism considered for the structure is a rotation around a pivot point located near the wall toe (Burland et al., 1981; Bowles, 1982; Padfield and Mair, 1984, Bolton and Powrie, 1987; Bica and Clayton, 1989; King, 1995; Osman and Bolton, 2004;

Peer review under responsibility of The Japanese Geotechnical Society.
* Corresponding author.
E-mail addresses: enrico.conte@ unical.it (E. Conte), antonello.troncone@unical.it (A. Troncone).

https://doi.org/10.1016/j.sandf.2018.08.012
0038-0806/

Madabhushi and Chandrasekaran, 2005; Gaba et al., 2017). Owing to this mechanism, it is assumed that the normal stresses above the pivot consist of active stresses on the retained side and passive stresses on the excavated side. Below the rotation point, soil goes from the active to the passive state, with passive stresses on the retained side. As a further simplification, the contact stress distribution shown in Fig. 1 is often considered, with the horizontal contact stresses below the rotation point, which are replaced by a resultant force, R, applied at this point (Blum, 1931). The required embedment depth is evaluated from the moment equilibrium about the same point, and the resulting depth is empirically increased by 20% in order to allow the development of R. Once this force is calculated from the equilibrium of the horizontal forces, it is also necessary to check whether the resulting embedment depth is sufficient to generate the force R under the action of the passive pressures behind the wall and the active pressures in front of it. This method was originally proposed by Blum (1931) and is commonly used in practice, especially in Europe. To analyse the behaviour of the wall under service conditions, a similar contact stress distribution is often used in conjunction with a safety factor that should overcome the uncertainties in the input parameters and ensure that the structure remains serviceable under working conditions (Burland et al., 1981; Valsangkar and Schriver, 1995; Powrie, 1996; Pane and Tamagnini, 1997). However, a drawback of this approach is that the resulting internal forces in the wall depend on the value of the safety factor and also on the particular way in which this safety factor is introduced into the calculations (Bolton et al., 1989).

In the present study, a simple to use method is proposed for the analysis of cantilever diaphragm walls in cohesive soils under undrained and drained conditions. In this method a rectilinear distribution of the net contact stresses is assumed at the soil-wall interface, the values of which are not completely predetermined by limit state. A similar distribution was also proposed by King (1995), Day (1999) and more recently by Conte et al. (2017), for analysing the behaviour of retaining walls embedded in dry sand. Simple equations are derived to calculate the contact stress distribution and the associated internal forces arising in the structure. These equations can be readily used to analyse the wall behaviour in ultimate and service conditions. Some comparisons with Blum's method are also carried out to show the usefulness of the proposed method for practical purposes.

2. Proposed method

Under the assumption that a structural failure does not occur, a cantilevered diaphragm wall generally moves as an approximately rigid body that rotates about a point located in proximity of the base of the structure (Fig. 2) owing to the soil excavation in front of it (Bolton and Powrie, 1987, 1988; Clough and O'Rourke, 1990). As a consequence of this mechanism, the soil and the wall undergo large displacements in their upper portion, and much smaller displacements in the lower portion. As an example, Fig. 3 shows the excavation-induced soil movements observed during a centrifuge test (Bolton and Powrie, 1988). It is clearly evident from this figure that the soil displacements significantly reduce near the base of the structure. In view of the above mechanism, it is reasonable to assume that, up to a certain depth from the excavation level, the wall is subjected to active stresses on the retained side and to passive stresses on the excavated side. Below the above-mentioned depth, however, the assumption that the contact stresses are at limit state is not appropriate, as it was documented in several experimental studies (Terzaghi, 1934; James and Bransby, 1970; Clayton and Milititsky, 1986).

The method proposed in this paper is based on this evidence and allows the behaviour of diaphragm walls in

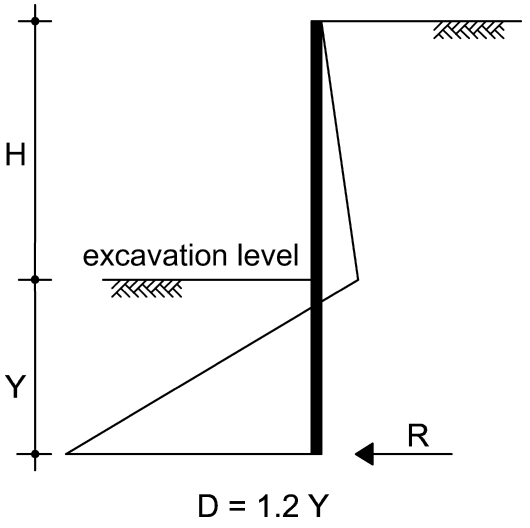

Fig. 1. Horizontal stress distribution assumed by Blum (1931).

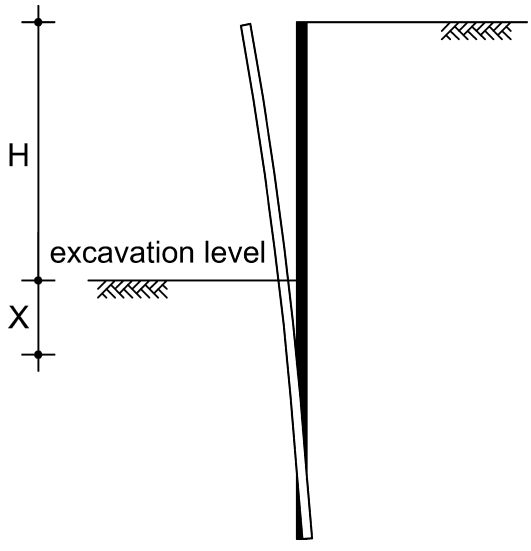

Fig. 2. Displacement pattern of a cantilevered diaphragm wall.

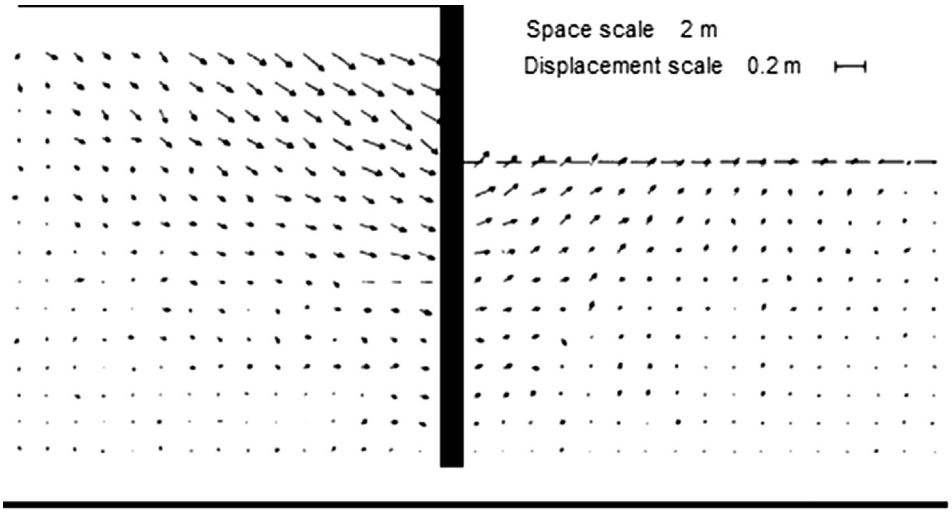

Fig. 3. Excavation-induced soil movements observed during a centrifuge test (modified from Bolton and Powrie, 1988).

cohesive soils to be analysed under both the undrained and drained conditions. A detailed description of this method is provided in the subsequent sections.

3. Diaphragm wall under undrained conditions

A diaphragm wall embedded in a purely cohesive soil with horizontal ground surface is schematized in Fig. 4. Height H and penetration D of the structure are assigned. The soil is completely saturated with unit weight γ, and undrained strength c_u. Considering that the installation of the wall generally produces some smear of the soil in contact with the wall, a resistance c_a (adhesion) is assumed at the soil-wall interface, with $c_a \leqslant c_u$. Therefore, the active and passive stresses σ_a and σ_p (in terms of total stress) at a given depth are approximately evaluated using the following equations (Rowe, 1957):

$$\sigma_a = \sigma_v - \alpha\, c_u \tag{1}$$

$$\sigma_p = \sigma_v + \alpha\, c_u \tag{2}$$

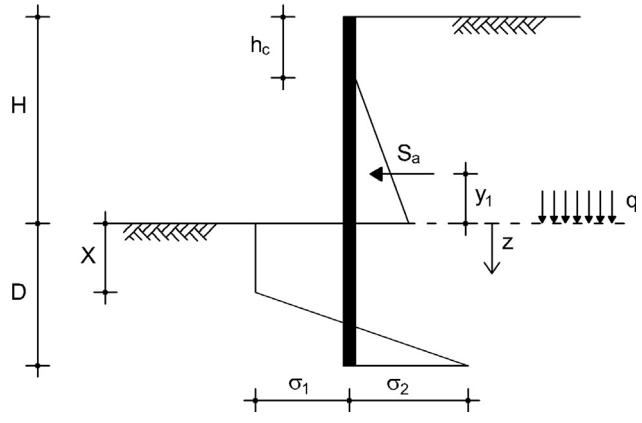

Fig. 4. Net horizontal stress distribution assumed in the proposed method for diaphragm walls in cohesive soils under undrained conditions.

where σ_v is the vertical total stress at that depth, and α is given by

$$\alpha = 2\sqrt{1 + \frac{c_a}{c_u}} \tag{3}$$

with $\alpha = 2$ when the adhesion effects are ignored.

Fig. 4 also shows the net horizontal stress diagram considered in the present study. Specifically, it is assumed that the soil above the excavation level is in an active limit state owing to the wall movement. In this connection, the value of σ_a at any depth is calculated using Eq. (1). The scheme of Fig. 4 also accounts for the presence of a vertical tension crack on the retained side, the depth of which is estimated as $h_c = \alpha\ c_u/\gamma$. For simplicity, the active stresses acting on the portion of wall with height $H - h_c$ are replaced by their resultant force S_a applied at a distance y_1 from the excavation level. The expression of S_a and y_1 are respectively:

$$S_a = \frac{1}{2}\,\gamma\,(H - h_c)^2 \tag{4}$$

$$y_1 = \frac{1}{3}\,(H - h_c) \tag{5}$$

In order to calculate the lateral stresses below the excavation level, it is convenient to treat the soil mass above this level as a surcharge $q = \gamma H$ (Fig. 4). Considering that, up to a depth X measured from the excavation level (Fig. 4), the active and passive stresses are fully mobilised behind and in front of the wall respectively, the net lateral stress (i.e. the difference between the passive stress and the active stress) acting on the portion of wall from the excavation level to depth X, is constant with depth and is given by

$$\sigma_1 = 2\,\alpha\, c_u - q \tag{6}$$

where $\sigma_1 > 0$, otherwise a wall with that height is impossible to be stable.

At depths greater than X, where the contact stresses are not at limiting conditions owing to a significant reduction of the soil displacements (Figs. 2 and 3), the net stress varies

linearly from σ_1 at depth X on the excavated side, to σ_2 at the wall toe on the retained side (Fig. 4). In other words, unlike the traditional methods based on the limit equilibrium approach (Blum, 1931; Padfield and Mair, 1984), the assumption of rigid-plastic behaviour of the soil is not maintained in the proposed method. It is also worth noting that the net stress diagram shown in Fig. 4 is completely defined once X and σ_2 are known. To this end, equating the horizontal forces acting on the wall and the moments generated by these forces about the wall toe, leads to a system of two equations from which the following expressions for X and σ_2 can be readily obtained (See Appendix A):

$$X = D - \frac{3}{2}\frac{[\sigma_1 D^2 - 2 S_a (y_1 + D)]}{(\sigma_1 D - S_a)} \tag{7}$$

$$\sigma_2 = \frac{4}{3}\frac{(\sigma_1 D - S_a)^2}{[\sigma_1 D^2 - 2 S_a (y_1 + D)]} - \sigma_1 \tag{8}$$

with $0 < X < D$ and σ_2 not exceeding a limit value, σ_{lim}, given by the difference between the passive stress and the active stress at the wall toe, i.e.

$$\sigma_{lim} = 2\alpha c_u + q \tag{9}$$

In other words, the net stress diagram shown in Fig. 4, with X and σ_2 calculated using Eqs. (7) and (8) respectively, can be employed for any assumed value of D provided that $0 < X < D$ and $\sigma_2 \leqslant \sigma_{lim}$. It is also worth noting that Eq. (8), in which it is imposed $\sigma_2 = \sigma_{lim}$, allows an evaluation of the minimum embedment necessary to ensure the wall stability, D_{min}. In this circumstance (i.e., when $\sigma_2 = \sigma_{lim}$), the proposed method coincides with the method developed by Bowles (1982), which is commonly used in the USA for the design of diaphragm walls.

Once X and σ_2 are known, the internal forces (i.e., shear force T, and bending moment, M) can be calculated at any depth. Considering that the internal forces in the portion of the wall above the excavation level are simple to be calculated, the expressions of T and M at depth z below the excavation level (Fig. 4) are only provided in the present paper. These expressions are:

– for $z \leqslant X$

$$T = -\sigma_1 z + S_a \tag{10}$$

$$M = -\sigma_1 \frac{z^2}{2} + S_a (y_1 + z) \tag{11}$$

– for $X \leqslant z \leqslant D$

$$T = S_a + \left(\frac{\sigma_1 + \sigma_2}{D - X}\right)\frac{(z - X)^2}{2} - \sigma_1 z \tag{12}$$

$$M = S_a (y_1 + z) + \left(\frac{\sigma_1 + \sigma_2}{D - X}\right)\frac{(z - X)^3}{6} - \sigma_1 \frac{z^2}{2} \tag{13}$$

4. Diaphragm wall under drained conditions

For cohesive soils under drained conditions, the active and passive effective stresses, σ'_a and σ'_p, acting on the wall in the horizontal direction, can be evaluated using the following equations:

$$\sigma'_a = K_a \sigma'_v - K_{ac} c' \tag{14}$$

$$\sigma'_p = K_p \sigma'_v + K_{pc} c' \tag{15}$$

where

$$K_{ac} = (1 - K_a)\,\mathrm{cotg}\phi' \tag{16}$$

$$K_{pc} = (K_p - 1)\,\mathrm{cotg}\phi' \tag{17}$$

σ'_v is the vertical effective stress at a given depth, K_a and K_p are respectively the active and passive earth pressure coefficients, c' is the effective cohesion and ϕ' is the shearing resistance angle of the soil. Eqs. (14)–(17) have been derived in the present study using the theorem of the corresponding states (Caquot, 1934) under the assumption that the effects of the adhesion at the soil-wall interface are negligible (See Appendix B for their derivation). In order to calculate the coefficients K_a and K_p appearing in these equations, the analytical expressions derived by Lancellotta (2002, 2008) can be used. These expressions are:

$$K_a = \left[\frac{\cos\delta}{1 + \sin\phi'}\left(\cos\delta - \sqrt{\sin^2\phi' - \sin^2\delta}\right)\right] e^{-2\vartheta_a \tan\phi'} \tag{18}$$

$$K_p = \left[\frac{\cos\delta}{1 - \sin\phi'}\left(\cos\delta + \sqrt{\sin^2\phi' - \sin^2\delta}\right)\right] e^{2\vartheta_p \tan\phi'} \tag{19}$$

with

$$2\vartheta_a = \sin^{-1}\left(\frac{\sin\delta}{\sin\phi'}\right) - \delta \tag{20}$$

$$2\vartheta_p = \sin^{-1}\left(\frac{\sin\delta}{\sin\phi'}\right) + \delta \tag{21}$$

and δ is the soil-wall friction angle the effect of which is hence accounted for in Eqs. (14)–(17),

As is well known, the pore water pressures acting on the wall under drained conditions can be calculated separately from the effective stresses. In order to evaluate these pressures when water flows through soil, the steady-state hydrodynamic equation is generally solved using some numerical techniques, such as the finite element method or the finite difference method. However, if the wall is impermeable and the hydraulic head is dissipated uniformly with depth, the pore water pressures on the wall can be readily calculated using an approximate solution in which a one-dimensional water flow is considered (Symons, 1983). This flow is characterized by a constant hydraulic gradient, i, that is a function of the total head difference, h, and the length of the submerged portion of the

wall on the excavated side, d (Fig. 5). The net pore water pressure distribution calculated using this approximate solution is shown in Fig. 5a and b for two possible situations, in which $i = h/(h + 2d)$ (Fig. 5a) and $i = h/(h + d + D)$ (Fig. 5b). In these figures, it is also indicated the maximum net pore water pressure, u_m, the expression of which is

$$u_m = \gamma_w h \frac{2d}{h + 2d} \tag{22}$$

or

$$u_m = \gamma_w h \frac{d + D}{h + d + D} \tag{23}$$

for the situation schematized in Fig. 5a and b, respectively. In these equations, γ_w is the unit weight of water. For simplicity but without loss of generality, the case considered in the present study is when the groundwater level is located at the ground surface, both on the retained side and the excavated side. In this circumstance, $h = H$ and $d = D$ are used in Eqs. (22) and (23), and the vertical effective stress at a given depth beneath the ground surface is

$$\sigma'_v = \gamma'_m z \tag{24}$$

on the retained side, and

$$\sigma'_v = \gamma'_v z \tag{25}$$

on the excavated side, where

$$\gamma'_m = \gamma' + i\gamma_w \tag{26}$$

$$\gamma'_v = \gamma' - i\gamma_w \tag{27}$$

and γ' is the effective unit weight of the soil.

To analyse the long term behaviour of a diaphragm wall, the profile of the net horizontal effective stress shown in Fig. 6 is considered. In the same figure, it is also plotted the assumed distribution of the net pore water pressure. The resultant force of the active stresses above the excavation level is again denoted as S_a with y_1 defining the position of its application point. In addition, the depth of the tension crack on the retained side is

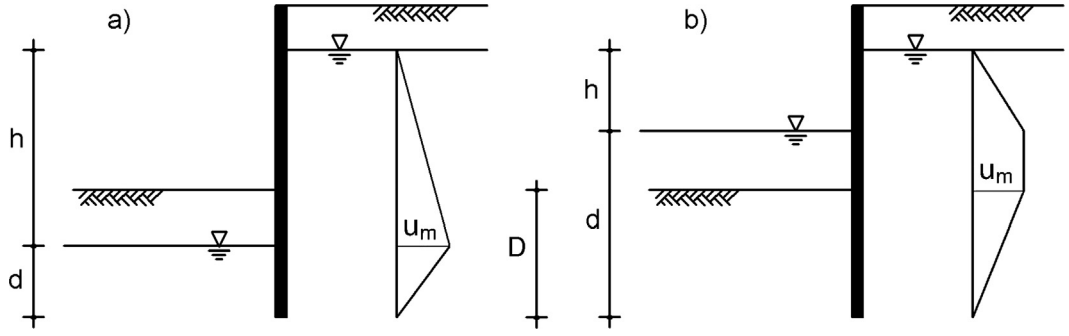

Fig. 5. Approximate net pore water pressure distributions on a diaphragm wall.

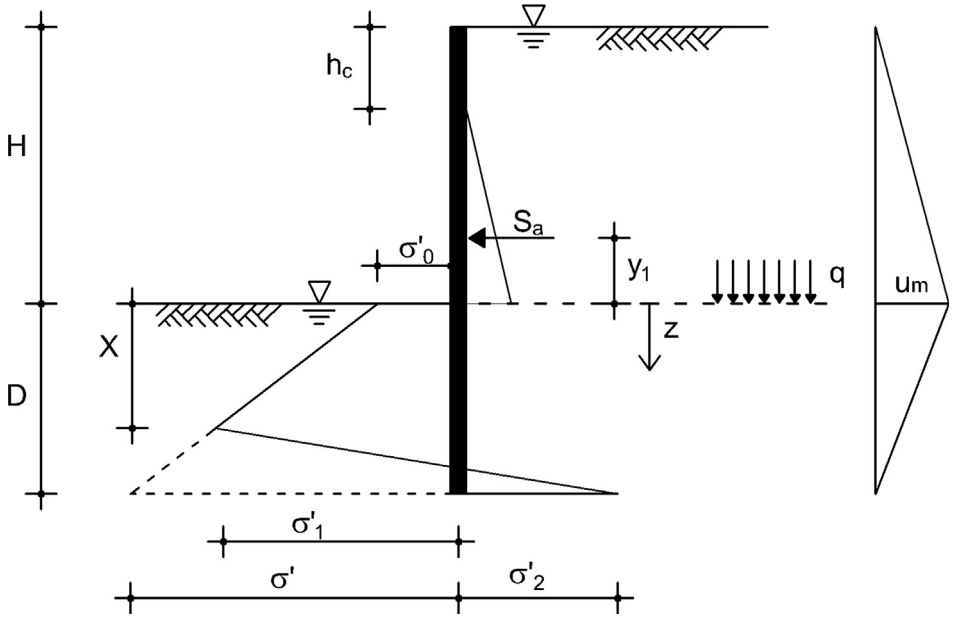

Fig. 6. Net horizontal stress distribution and net pore water pressure distribution assumed in the proposed method for diaphragm walls in cohesive soils under drained conditions, when $c' \geqslant \frac{K_a q}{K}$.

$$h_c = \frac{K_{ac}\, c'}{K_a\, \gamma'_m} \tag{28}$$

Depth X defines again the extension of the plastic zone (measured from the excavation level) where the active and passive stresses are fully mobilized. The net stress distribution on this portion of wall is linear with a gradient given by $(K_p\,\gamma'_v - K_a\,\gamma'_m)$ and the net horizontal effective stress σ'_o at the excavation level (i.e. at $z = 0$) is

$$\sigma'_o = K\,c' - K_a\,q \tag{29}$$

where $K = K_{ac} + K_{pc}$ and $q = \gamma'_m H$. Although the scheme shown in Fig. 6 refers to the case when $c' \geqslant \frac{K_a q}{K}$, the equations presented below can be also used when $c' < \frac{K_a q}{K}$ (Fig. 7). In Figs. 6 and 7, the net horizontal effective stress σ'_1 at depth X, and the net horizontal effective stress σ' at the wall end on the excavated side, are also shown. The expressions of these net stresses are:

$$\sigma'_1 = (K_p\,\gamma'_v - K_a\,\gamma'_m)\,X + \sigma'_o \tag{30}$$

and

$$\sigma' = (K_p\,\gamma'_v - K_a\,\gamma'_m)\,D + \sigma'_o \tag{31}$$

At depths greater than X, it is assumed that the net lateral effective stress varies linearly from σ'_1 at depth X to σ'_2 at the wall toe. The unknown quantities X and σ'_2 can be calculated from the equilibrium conditions of the wall (including the pore water pressure contribution). The resulting expressions of X and σ'_2 (obtained using a similar procedure to that described in Appendix A) are respectively:

$$X = D - \frac{(\sigma' + 2\,\sigma'_o)\,D^2 - 6\,[S_a\,(y_1 + D) + S_w\,y_w]}{[(\sigma' + \sigma'_o)\,D - 2\,(S_a + S_w)]} \tag{32}$$

$$\sigma'_2 = \frac{[(\sigma' + \sigma'_o)\,D - 2\,(S_a + S_w)]^2}{(\sigma' + 2\,\sigma'_o)\,D^2 - 6\,[S_a\,(y_1 + D) + S_w\,y_w]} - \sigma' \tag{33}$$

with $0 < X < D$ and $\sigma'_2 \leqslant \sigma'_{lim}$, where

$$\sigma'_{lim} = (K_p\,\gamma'_m - K_a\,\gamma'_v)\,D + K_p\,q + K\,c' \tag{34}$$

S_w is the resultant of the net pore water pressures acting on the wall and y_w defines the position of the application point of S_w from the wall toe. The terms S_w and $S_w\,y_w$ appearing in Eqs. (32) and (33) are expressed by

$$S_w = \frac{1}{2}\,u_m\,(H + D) \tag{35}$$

$$S_w\,y_w = \frac{1}{6}\,u_m\,(H^2 + 3HD + 2D^2) \tag{36}$$

In addition, the internal forces at a depth z measured from the excavation level, are given by the following equations:

– for $z \leqslant X$

$$T = -\frac{1}{2}\,(K_p\,\gamma'_v - K_a\,\gamma'_m)\,z^2 - \sigma'_o\,z + S_a + T_w \tag{37}$$

$$M = -\frac{1}{6}\,(K_p\,\gamma'_v - K_a\,\gamma'_m)\,z^3 - \frac{1}{2}\sigma'_o\,z^2 + S_a\,(y_1 + z) + M_w \tag{38}$$

– for $X \leqslant z \leqslant D$

$$T = \left(\frac{\sigma'_1 + \sigma'_2}{D - X}\right)\frac{(z - X)^2}{2} - \sigma'_1\,(z - X) + S_a - \left(\frac{\sigma'_o + \sigma'_1}{2}\right)X + T_w \tag{39}$$

$$M = \left(\frac{\sigma'_1 + \sigma'_2}{D - X}\right)\frac{(z - X)^3}{6} - \sigma'_1\frac{(z - X)^2}{2} + S_a\,(y_1 + z) + - \left[\sigma'_o X\left(z - \frac{X}{2}\right) + \left(\frac{\sigma'_1 - \sigma'_o}{2}\right)X\left(z - \tfrac{2}{3}X\right)\right] + M_w \tag{40}$$

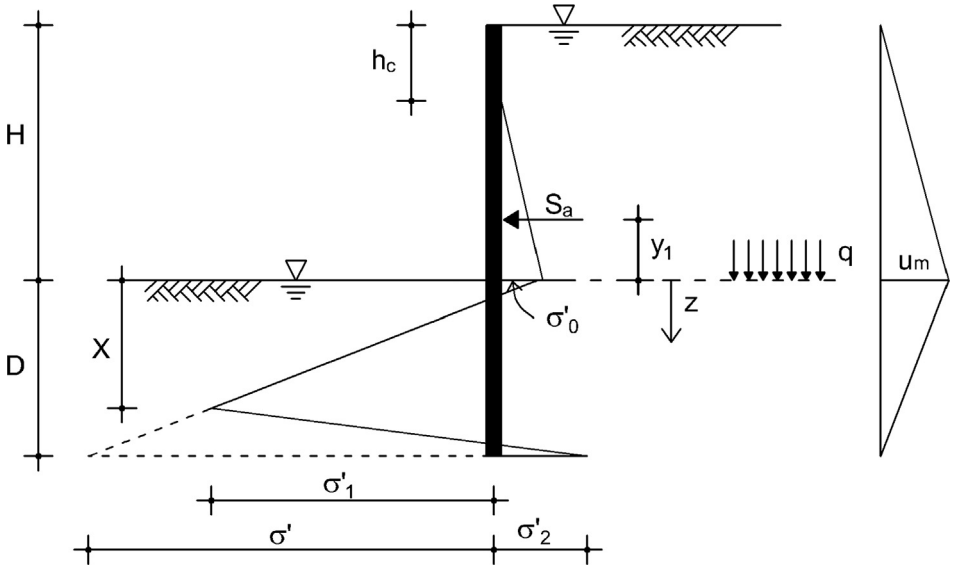

Fig. 7. Net contact stress distribution and net pore water pressure distribution assumed in the proposed method for diaphragm walls in cohesive soils under drained conditions, when $c' < \frac{K_a q}{K}$.

where T_w and M_w are the shear force and the bending moment at depth z due to the pore water pressures acting on the wall. For the net pore pressure profile shown in Figs. 6 and 7, T_w and M_w are

$$T_w = \frac{1}{2}\, u_m H + u_m \left(1 - \frac{z}{2D}\right) z \tag{41}$$

$$M_w = \frac{1}{2}\, u_m H \left(\frac{H}{3} + z\right) + \frac{u_m}{2} \left(1 - \frac{z}{3D}\right) z^2 \tag{42}$$

Finally, it must be noted that, for both drained and undrained conditions, a factor of safety can be calculated as the reduction factor of the soil strength parameters which determines a condition of incipient collapse of the wall (i.e., when $\sigma_2 = \sigma_{lim}$ under undrained conditions, or $\sigma'_2 = \sigma'_{lim}$ under drained conditions).

5. Limitations of the proposed method

The proposed method can be used for the preliminary design of a cantilever diaphragm wall that moves as an essentially rigid body rotating around a point located near the base of the structure. In view of this behaviour, it is assumed that the net normal stresses acting on the wall are at limit state (active on the retained side/passive on the excavated side) up to a depth X measured from the excavation level (Figs. 4 and 6). In particular, for diaphragm walls under drained conditions, these stresses can be readily calculated using some existing solutions (Janbu, 1972; Caquot and Kerisel, 1948) or the equations suggested in the present paper for the case of vertical and rough walls and horizontal ground surface. Some simple solutions are also reported for evaluating approximately the net pore water pressures acting on the wall, under the assumptions of impermeable wall and water seepage with constant gradient. Below depth X, it is assumed that the net normal stress varies linearly with depth and attains an unknown value (σ_2 or σ'_2) at the wall base, on the retained side (Figs. 4 and 6). The above-mentioned wall mechanism (a rigid rotation) generally occurs when the embedment length, D, is not excessively long. From an analytical point of view, this condition is met when, for an assigned value of D (with $D > D_{min}$), the calculated depth X falls into the range $0 < X < D$, and the calculated net normal stress at the wall base (σ_2 or σ'_2) is not greater than the respective net normal stress at the limit state (i.e., $\sigma_2 \leqslant \sigma_{lim}$ or $\sigma'_2 \leqslant \sigma'_{lim}$). These limitations define the field of applicability of the proposed method for the design of cantilever diaphragm walls.

5.1. Comparison with experimental data

To validate the proposed method, some comparisons with experimental data are shown in Figs. 8 and 9 in terms of bending moment distribution with depth. These data were obtained by King (1995) and Madabhushi and Zeng (2006) from centrifuge tests on diaphragm walls embedded in cohesionless soils. Unfortunately, the authors are not aware of similar results concerning walls in cohesive soils. In both case studies, the wall underwent a rotation about a point located in proximity of its base, consistently with the main assumption on which the present method is based.

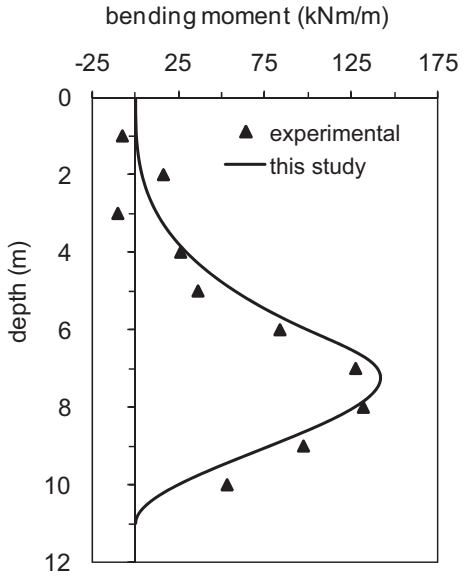

Fig. 8. Comparison between the bending moment distribution calculated using the present method and the values of the bending moment measured by King (1995) during a centrifuge test.

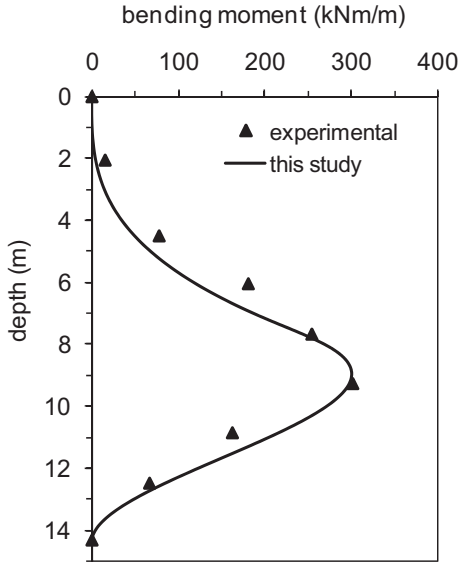

Fig. 9. Comparison between the bending moment distribution calculated using the present method and the values of the bending moment measured by Madabhushi and Zeng (2006) during a centrifuge test.

The case considered by King (1995) concerns a diaphragm wall with an excavation height of 6 m and an embedment length of 5 m. The wall was embedded in a sand with $\gamma = 14.2\ kN/m^3$ and $\phi' = 40°$. In addition, $\delta = 15.8°$. These data were obtained by King (1995) from the results of plane strain and direct shear tests. The soil

used in the tests by Madabhushi and Zeng (2006) was a fine sand with a relative density of 92%. The input data for this case study are $H = 7.2$ m, $D = 7.2$ m, $\gamma = 16.4$ kN/m^3, $\phi' = 40°$ and $\delta = 12°$ (See also Conti and Viggiani, 2013). As can be seen from Figs. 8 and 9, there is good agreement between the bending moment diagram calculated using the proposed method and the available experimental data. Other comparisons with numerical and experimental results concerning diaphragm walls embedded in cohesionless soils can be found in Conte et al. (2017).

6. Comparison with the limit equilibrium method

In this section, some comparisons with the classical method developed by Blum (1931) are presented to show the usefulness of the proposed method for practical purposes. Although Blum's method was proposed many years ago, it is still extensively used in many countries of the world, especially in Europe. A description of this method has been provided in a precedent section of the present paper. A diaphragm wall with $H = 6$ m is considered as an example. The assumed soil properties are $\gamma = 20$ kN/m^3, $c_u = 40$ kPa, $c' = 5$ kPa and $\phi' = 26°$. In addition, it is assumed that $\delta = 20°$ and the adhesion effects are ignored. For this wall, three conditions are considered: (1) the soil is completely saturated and the analysis is performed under undrained conditions (*Case A*). (2) The soil is completely saturated with the groundwater level at the ground surface (both on the retained side and on the excavated side), and the analysis is performed under drained conditions (*Case B*). In this connection, the approximate solution previously described in the present paper is used to evaluate the net pore water pressure distribution due to the steady-state seepage from the ground surface on the retained side into the soil below the excavation level. (3) A drained analysis is again performed, but it is assumed that the groundwater level is at the excavation level both on the retained side and the excavated side (*Case C*). In this latter case, no water flow occurs and the net water pressure is zero at any depth. A different unit weight is, however, used for the soil above and below the excavation level, i.e. γ and γ' respectively.

The minimum embedment length D_{min} is first calculated using the present method. The resulting values are shown in Table 1 for each case study considered. As expected, the most critical condition for the wall stability is the long term one when the soil is completely saturated and a steady-state flow occurs (*Case B*). In this case, in fact, a much higher value of D_{min} (9.10 m) is required to ensure stability. Different values of the embedment length D are then assumed (with $D > D_{min}$) to show the influence of this parameter on the lateral stress distribution and the internal forces of the wall. In this connection, the depth X and the net horizontal stress at the wall toe (σ_2 for *Case A*, or σ'_2 for *Cases B* and *C*) are calculated using the equations derived in the present study (Eqs. (7) and (8) or Eqs. (32) and (33)), and the respective results are shown in Figs. 10 and 11 as a function of D. As can be seen, all the above parameters increase with decreasing D. In other words, the smaller the embedment length, the deeper the extension of the plastic zone below the excavation level (Fig. 10) and the higher the net normal stress at the wall toe (Fig. 11). The results of Figs. 10 and 11 (along with the data in Table 1) also define the range of the possible values of D for which the proposed method can be used for each case study considered.

Finally, Figs. 12–15 compare the bending moment and shear force distributions predicted by Blum's method and those calculated using the present method, for some values of D. The sign convention used for the bending moment and shear force is indicated in Fig. 12. As expected, the results provided by the above-mentioned methods (both

Table 1
Minimum embedment length D_{min} calculated using the present method for the considered case studies.

Case	D_{min} (m)
A	2.68
B	9.10
C	4.95

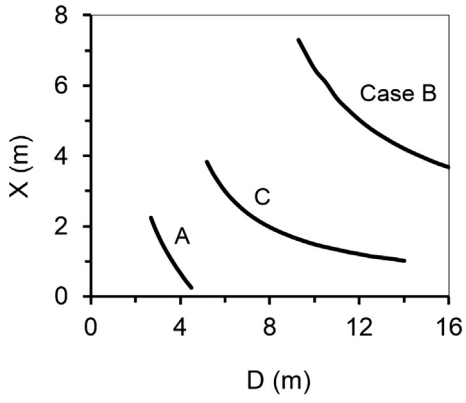

Fig. 10. Effect of the embedment length D on the extension of the plastic zone, X.

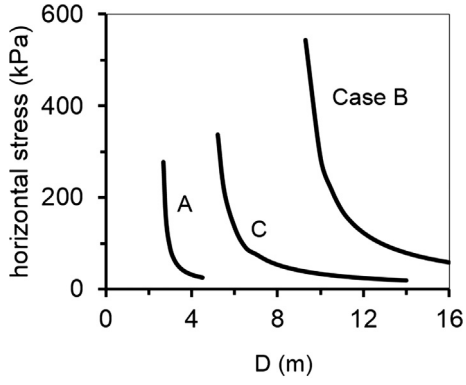

Fig. 11. Effect of the embedment length D on the net horizontal stress at the wall toe (i.e., σ_2 for *Case A*, or σ'_2 for *Cases B* and *C*).

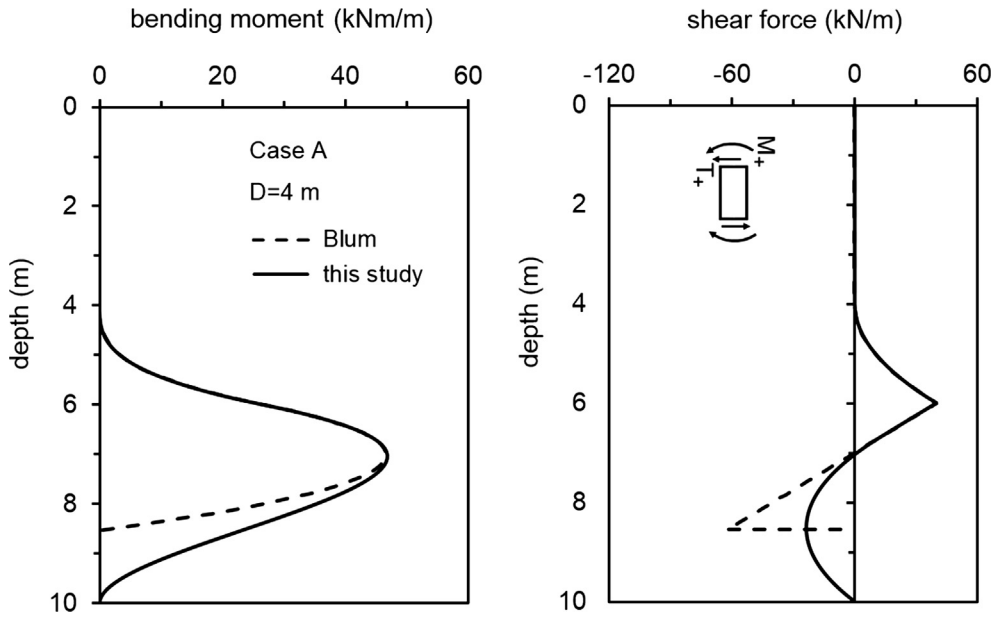

Fig. 12. Bending moment and shear force distributions calculated using the present method and Blum's method for *Case A* when $D = 4$ m. The sign convention used for the shear force and bending moment is also indicated.

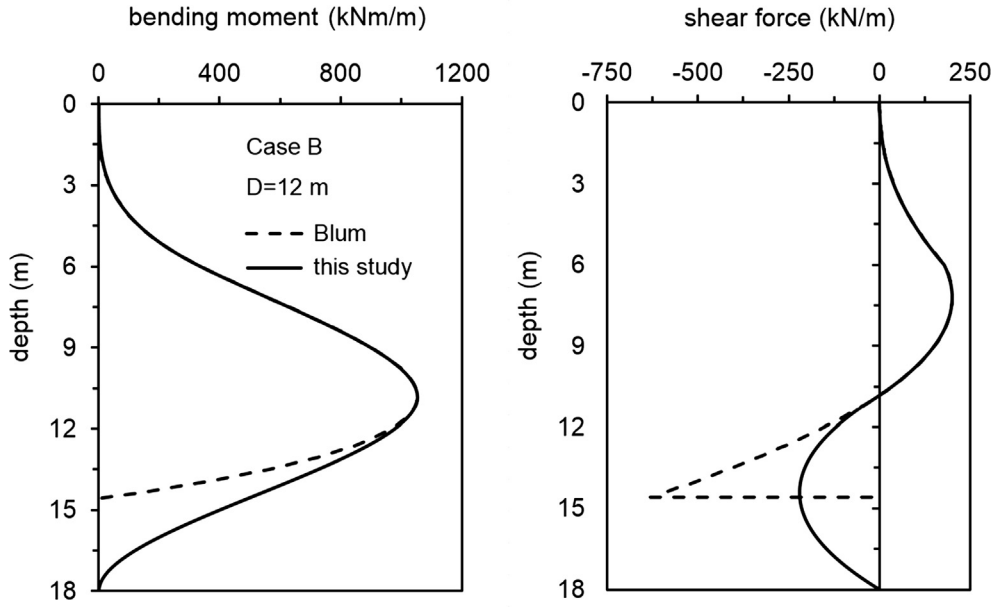

Fig. 13. Bending moment and shear force distributions calculated using the present method and Blum's method for *Case B* when $D = 12$ m.

in terms of bending moment and shear force) are coincident in the upper portion of the wall. At greater depths, however, the internal forces are rather different, both in magnitude and trend. Blum's method generally provides a good estimation of the maximum bending moment, but it could underestimate this internal force when D is significantly greater than D_{min} (Fig. 15). Another drawback of Blum's method is that it provides the same results (both in terms of bending moment and shear force) irrespective of the value of D (Figs. 14 and 15). It is also worth noting that Blum's method considerably overestimates the maximum shear force and could lead to unsustainable values of this internal force (Figs. 13–15).

In summary, as Blum's method (as well as other similar methods based on the limit equilibrium concept) refers to an incipient failure condition of the wall (when $D = D_{min}$), the contact stresses and the internal forces calculated using this method do not change with changes in D (with $D > D_{min}$). In addition, in the lower portion of the wall, Blum's method provides values of the internal forces (especially the shear force) that are not realistic. These drawbacks can be overcome using the proposed

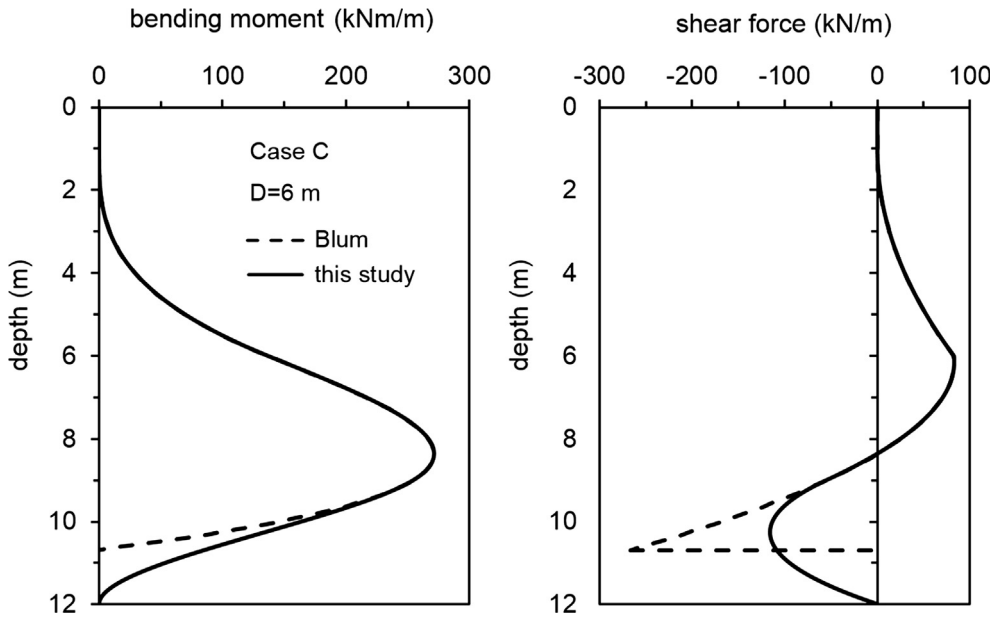

Fig. 14. Bending moment and shear force distributions calculated using the present method and Blum's method for *Case C* when $D = 6$ m.

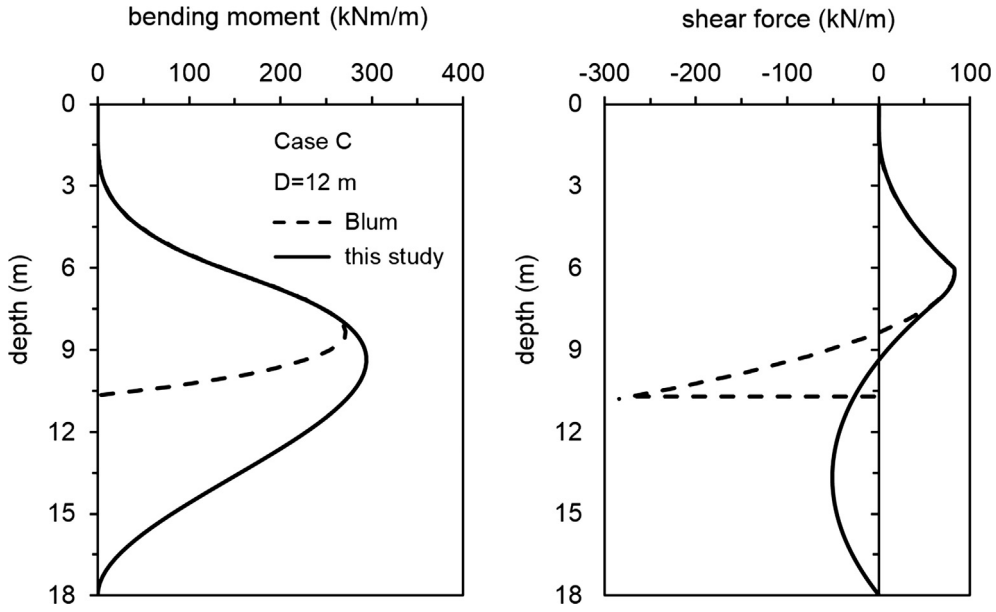

Fig. 15. Bending moment and shear force distributions calculated using the present method and Blum's method for *Case C* when $D = 12$ m.

method that hence represents a reliable alternative to the conventional methods.

7. Concluding remarks

A method has been proposed for a simplified analysis of diaphragm walls in cohesive soils under undrained and drained conditions. In this method, it is assumed that the wall moves as an approximately rigid body rotating around a point located in proximity to its base. Due to this movement, a rectilinear distribution of the net contact stresses not predetermined by the limit state is considered at the soil-wall interface. Simple equations have been derived to calculate the contact stresses and the associated internal forces arising in the structure. These equations can be easily implemented in a common spreadsheet to readily analyse the wall behaviour in the ultimate and service conditions. Moreover, few parameters are required as input data.

The proposed method overcomes the limitations of the conventional design methods based on the limit equilibrium approach and is hence a reliable alternative to these methods. In this connection, some comparisons have been carried out between the present method and Blum's method which is widely used in practice. The results, in terms of the bending moment and shear force provided

by these methods, are coincident in the upper portion of the wall. At greater depths, however, the calculated values of the internal forces could differ considerably both in magnitude and trend. Specifically, Blum's method grossly overestimates the maximum shear force and could underestimate the maximum bending moment when the embedment length of the wall is significantly higher than the minimum value required for ensuring wall stability.

Appendix A. *A.1. Calculation of depth X and net lateral stress σ_2 in cohesive soils under undrained conditions*

With reference to Fig. 4, the equilibrium equation for the horizontal forces acting on the wall can be written as:

$$S_a + (\sigma_1 + \sigma_2)\,\frac{y}{2} - \sigma_1 D = 0 \tag{A-1}$$

where $y = D - X$. In addition, moment equilibrium about the wall toe gives

$$S_a\,(y_1 + D) + (\sigma_1 + \sigma_2)\,\frac{y^2}{6} - \sigma_1\,\frac{D^2}{2} = 0 \tag{A-2}$$

Solving Eq. (A-1) for y yields

$$y = 2\,\frac{\sigma_1 D - S_a}{(\sigma_1 + \sigma_2)} \tag{A-3}$$

and substituting Eq. (A-3) into Eq. (A-2) leads to the following expression for σ_2:

$$\sigma_2 = \frac{4}{3}\,\frac{(\sigma_1 D - S_a)^2}{[\sigma_1 D^2 - 2 S_a\,(y_1 + D)]} - \sigma_1 \tag{A-4}$$

Finally, after substituting Eq. (A-4) into Eq. (A-3) and taking into account that $X = D - y$, the expression of X can be also obtained, i.e.

$$X = D - \frac{3}{2}\,\frac{[\sigma_1 D^2 - 2 S_a\,(y_1 + D)]}{(\sigma_1 D - S_a)} \tag{A-5}$$

Appendix B. *B.1. Calculation of the active and passive effective stresses σ'_a and σ'_p in cohesive soils*

Consider a vertical wall that sustains a horizontal backfill. It is assumed that the soil obeys the Morh-Coulomb failure criterion with strength parameters c' and ϕ', and the wall is rough with friction angle δ whereas adhesion is nil. In accordance with the theorem of the corresponding states (Caquot, 1934), an ideal soil having the same value of ϕ' but with $c' = 0$ is considered. However, an uniform surcharge q^* is applied at the boundary of this ideal soil (i.e., at the ground surface and the soil-wall interface), where

$$q^* = c'\,\mathrm{cotg}\,\phi' \tag{A-6}$$

With reference to this ideal soil, the active and passive stresses, σ'_a and σ'_p, acting on the wall in the horizontal direction, are expressed by the following equations:

$$\sigma'_a = K_a\,\sigma'_v + K_a\,q^* - q^* \tag{A-7}$$

$$\sigma'_p = K_p\,\sigma'_v + K_p\,q^* - q^* \tag{A-8}$$

where σ'_v is the vertical effective stress at a given depth, K_a and K_p are the active and passive earth pressure coefficients that depend on ϕ' and δ. These coefficients can be calculated using the analytical expressions derived by Lancellotta (2002, 2008). Substituting Eq. (A-6) into Eqs. (A-7) and (A-8) leads to the following equations:

$$\sigma'_a = K_a\,\sigma'_v - K_{ac}\,c' \tag{A-9}$$

$$\sigma'_p = K_p\,\sigma'_v + K_{pc}\,c' \tag{A-10}$$

where

$$K_{ac} = (1 - K_a)\,\mathrm{cotg}\phi' \tag{A-11}$$

and

$$K_{pc} = (K_p - 1)\,\mathrm{cotg}\phi' \tag{A-12}$$

Similarly, the equations for calculating the associated contact stresses in the vertical direction can be derived. They take the form:

$$\sigma'_{av} = K_a\,\mathrm{tg}\delta\,(\sigma'_v + c'\,\mathrm{cotg}\phi') \tag{A-13}$$

$$\sigma'_{pv} = K_p\,\mathrm{tg}\delta\,(\sigma'_v + c'\,\mathrm{cotg}\phi') \tag{A-14}$$

References

Bica, A.V.D., Clayton, C.R.I., 1989. Limit equilibrium design methods for free embedded cantilever walls in granular materials. Proc. Inst. Civ. Eng. Part 1 86, 879–989.

Blum, H., 1931. Einspannungsverhaltnisse bei Bohlkwerken. Ernst und Sohn, Berlin, Wil.

Bolton, M.D., Powrie, W., 1987. Collapse of diaphragm walls retaining clay. Géotechnique 37 (3), 335–353.

Bolton, M.D., Powrie, W., 1988. Behaviour of diaphragm walls in clay prior to collapse. Géotechnique 38 (2), 167–189.

Bolton, M.D., Powrie, W., Symons, I.F., 1989. The design of stiff in-situ walls retaining overconsolidated clay, Part I - Short term behaviour. Ground Eng. 22 (8/9), 34–47.

Bowles, J.E., 1982. Foundation Analysis and Design, third ed. McGraw-Hill, New York.

Burland, J.B., Potts, D.M., Walsh, N.M., 1981. The overall stability of free and propped embedded cantilever retaining walls. Ground Eng. 14 (5), 28–37.

Caquot, A., 1934. Equilibre des massifs a frottement interne. Stabilité des terres pulvérulents ou cohérentes, Guathier-Villars, Paris.

Caquot, A., Kerisel, J., 1948. Tables for the Calculation of Passive Pressure. Gauthier-Villars, Paris.

Clayton, C.R.I., Milititsky, J., 1986. Earth Pressure and Earth Retaining Structures. Surrey University Press, London.

Clough, G.W., O'Rourke, T.D., 1990. Construction induced movements of in situ walls. In: Lambe, P.C., Hansen, L.A. (Eds.), Design and Performance of Earth Retaining Structures, Geotechnical Special Publication No. 25. American Society of Civil Engineers, New York, NY, USA, pp. 430–470.

Conte, E., Troncone, A., Vena, M., 2013. Nonlinear three-dimensional analysis of reinforced concrete piles subjected to horizontal loading. Comput. Geotech. 49, 123–133.

Conte, E., Troncone, A., Vena, M., 2015. Behaviour of flexible piles subjected to inclined loads. Comput. Geotech. 69, 199–209.

Conte, E., Troncone, A., Vena, M., 2017. A method for the design of embedded cantilever retaining walls under static and seismic loading. Géotechnique 67 (12), 1081–1089.
Conti, R., Viggiani, G.M.B., 2013. A new limit equilibrium method for the pseudostatic design of embedded cantilevered retaining walls. Soil Dyn. Earthquake Eng. 50, 143–150.
Day, R.A., 1999. Net pressure analysis of cantilever sheet pile walls. Géotechnique 49 (2), 231–245.
Gaba, A., Hardy, S., Doughty, L., Powrie, W., Selemetas, D., 2017. Embedded Retaining Walls Guidance for Design Report C760. Construction Industry Research and Information Association, London.
James, R.G., Bransby, P.L., 1970. Experimental and theoretical investigations of a passive earth pressure problem. Géotechnique 20 (1), 17–37.
Janbu, N., 1972. Earth Pressures Computations in Theory and Practice. ECSMFE, Madrid.
King, G.J.W., 1995. Analysis of cantilever sheet-pile walls in cohesionless soil. J. Geotech. Eng., ASCE 121 (9), 629–635.
Lancellotta, R., 2002. Analytical solution of passive earth pressure. Géotechnique 52 (8), 617–619.
Lancellotta, R., 2008. Geotecnica, third ed. Zanichelli, Bologna, Italy.
Madabhushi, S.P.G., Chandrasekaran, V.S., 2005. Rotation of cantilever sheet pile walls. J. Geotech. Geoenviron. Eng., ASCE 131 (2), 202–212.
Madabhushi, S.P.G., Zeng, X., 2006. Seismic response of flexible cantilever retaining walls with dry backfill. Geomech. Geoeng. 1 (4), 275–289.
Osman, A.S., Bolton, M.D., 2004. A new design method for retaining walls in clay. Can. Geotech. J. 41, 451–466.
Padfield, C.J., Mair, R.J., 1984. Design of Retaining Walls Embedded in Stiff Clays Report 104. Construction Industry Research and Information Association, London.
Pane, V., Tamagnini, C., 1997. Problemi generali della analisi delle opera di sostegno. In: IV CNRIG: Il modello geotecnico del sottosuolo nella progettazione delle opere di sostegno e degli scavi, vol. II. Gruppo Nazionale di Coordinamento degli Ingegneria Geotecnica del CNR, Roma, Perugia, Italy, pp. 7–120.
Powrie, W., 1996. Limit equilibrium analysis of embedded retaining walls. Géotechnique 46 (4), 709–723.
Rowe, P.W., 1957. Sheet pile walls in clay. Proc. Inst. Civ. Eng. 7, 629–654.
Symons, I.F., 1983. Assessing the stability of a propped in-situ retaining wall in overconsolidated clay. Proc. Inst. Civ. Eng. Part 2 75, 617–633.
Terzaghi, K., 1934. Large retaining wall tests. I. Pressure of dry sand. Eng. News-Rec., 136–140
Valsangkar, A.J., Schriver, A.B., 1995. Partial and total factors of safety in anchored sheet pile design. Can. Geotech. J. 28, 812–817.